DOI: 10.1002/((please add manuscript number))

Article type: Full Paper

A High-Volumetric-Capacity Cathode Based on Interconnected Close-packed N-Doped Porous Carbon Nanospheres for Long-life Lithium–Sulfur Batteries

*Cheng Hu, Caroline Kirk, Qiong Cai, Carlos Cuadrado-Collados, Joaquín Silvestre-Albero, Francisco Rodríguez-Reinoso and Mark James Biggs**

Dr. C Hu, Prof. M. J. Biggs
School of Science
Loughborough University
Loughborough LE11 3TU, United Kingdom.
E-mail: m.biggs@lboro.ac.uk
Dr. C Kirk
Department of Chemistry
Loughborough University
Loughborough LE11 3TU, United Kingdom.
Dr. Q. Cai
Department of Chemical and Process Engineering
University of Surrey
Guildford GU2 7XH, United Kingdom
C. Cuadrado-Collados, Dr. J. Silvestre-Albero, Prof. F. Rodríguez-Reinoso
Laboratorio de Materiales Avanzados
Departamento de Química Inorgánica
Universidad de Alicante
Apartado 99 E-03080, Spain.

Keywords: Li-S battery, high volumetric capacity, monodisperse, interconnected carbon nanospheres, close-packed

We report a Li-S battery cathode of high volumetric-capacity enabled by novel micro- and meso-structuring. The cathode is based on monodisperse highly porous carbon nanospheres derived from a facile template- and surfactant-free method. At the mesoscale, the nanospheres structure into interconnected close-packed clusters of a few microns in extent, thus facilitating the fabrication of dense crack-free high areal sulfur loading (5 mg cm^{-2}) cathodes with high electrical conductivity and low cathode impedance. A combination of the nitrogen doping (5 wt%), high porosity (2.3 cm^3 g^{-1}) and surface area (2900 m^2 g^{-1}) at the microscale enables high sulfur immobilization and utilization. The cathode delivers amongst the best reported volumetric capacity to date, above typical Li-ion areal capacity at 0.2C over 200 cycles and low capacity fading of 0.1% per cycle at 0.5C over 500 cycles. The compact cathode structure also ensures a low electrolyte requirement (6 µL mg^{-1}), which aids a low overall cell weight, and further, amongst the best gravimetric capacities published to date as well.

1. Introduction

The need for batteries with high energy storage capacities is more important than ever before. Lithium-sulfur (Li-S) batteries are among the most promising systems due to the high theoretical specific capacity (1672 mAh g^{-1})[1] and the low cost of sulfur. On a volume-for-volume basis , Li-S batteries are expected to deliver at least the same energy as Li-ion batteries whilst being substantially cheaper and lighter.[2] They are, therefore, of great interest for replacing Li-ion technology in applications such as electric vehicles, mobile electronic devices, and aerospace and space applications.

Li-S batteries face challenges that originate from the properties of sulfur and products that arise along the battery charge/discharge route. Both sulfur and Li_2S (the final discharge product) are electrically insulating, whilst the low density of the latter, relative to sulfur, means significant volume expansion occurs within the cathode as discharge proceeds. These lead to a decline in sulfur utilization and, therefore, cell capacity over extended charge/discharge cycles. A further issue is the so-called “shuttle effect”, where electrolyte-soluble lithium polysulfide (LiPS) intermediates migrate between the anode and cathode, leading to a gradual degradation of the anode and cathode.[3-6] As a result of these issues, earlier Li-S batteries suffered from rapid capacity fading and poor Coulombic efficiency.[7, 8] In the past few years, compositing sulfur with porous carbon nano-particles has been found to be an effective solution to address the issues outlined above.[9-18] The nano-pores host sulfur in a conductive network whilst providing strong retention of the soluble LiPS. Use of nano-sized particles improves electrolyte-cathode contact and facilitates Li-ion diffusion, leading to a better (*i.e.* lower) cathode impedance.[19]

One of the remaining barriers to commercialization of Li-S batteries is achieving high overall gravimetric and volumetric capacities at sufficient areal sulfur loading within a reasonable cost

envelope.[20, 21] To be competitive with state-of-the-art commercial Li-ion batteries, areal sulfur loadings of at least 4-6 mg cm^{-2} are required.[20, 22, 23] In comparison, much of the prior work based on carbon nano-particles have been demonstrated using considerably lower sulfur loadings.[20] This is likely due to the challenges faced in forming a uniform thick coating of these nano-particulate carbon-sulfur composites on the current collector surface.[23]

Recently, sulfur loadings in excess of 10 mg cm^{-2} have been achieved by incorporating sulfur into 3D interconnected carbon networks.[24-28] Initial sulfur specific capacities beyond 800 mAh g^{-1} have now been achieved in such cases for cycling rates below 0.2C. However, just a few demonstrated long-term cycling at and above 0.5C.[29] Additionally, in order to improve sulfur utilization in these high sulfur-loading cathodes, loose macroporous structures have been employed by some.[27-29] This, however, leads to reduced volumetric capacity and elevated cell weight due to the high electrolyte fraction required to fill the macropores.

Whilst efforts have been expended to maximize areal sulfur loading so as to improve the areal capacity,[24-26, 28] very high areal sulfur loadings have been found to cause severe anode corrosion and consequent early cell failure.[28] A 4-6 mg cm^{-2} sulfur Li-S battery is of commercial interest to replace current Li-ion batteries provided that it can balance battery life time with volumetric and gravimetric capacity.[20]

In this contribution, we report on a Li-S cathode with long-life high performance for charge/discharge rates of up to 0.5C. The cathode is built upon highly porous and monodisperse nitrogen-doped carbon nanospheres (NCNS). The carbon was synthesized from template- and surfactant-free phenol resin precursors. A cathode composite was formed by incorporating 70 wt% of sulfur into 30 wt% of the NCNS using melt-diffusion method. The composite (NCNS-S70) exists as close-packed interconnected nanosphere clusters that enable the fabrication of a crack-

free compact cathode with high sulfur loading (5 mg cm^{-2}) using a conventional slurry coating method. The high surface area (BET 2900 m^2 g^{-1}) and porosity (total pore volume 2.3 cm^3 g^{-1}) of the NCNS provides excellent LiPS adsorbability. The voids between the nanospheres and their clusters were found to provide a balance between good ion diffusion and low electrolyte fraction, leading to high volumetric and overall cell gravimetric capacities.

2. Results and Discussion

2.1 Structure of the NCNS and NCNS-S70

To synthesize the NCNS (details available in Experimental Section), monodisperse phenol resin nano-spheres (PRNS) were first prepared following Zhao *et. al.*[30] The obtained PRNS suspension was then subjected to centrifugation to yield large-scale close-packed clusters of the PRNS (**Figure 1**a). The NCNS were then derived from the PRNS *via* carbonization, CO_2 activation and, finally, NH_3 nitrogenation.

Figure 1b-c shows the scanning electron microscopy (SEM) image of the as-synthesized NCNS. The high magnification SEM image in Figure 1c shows that the carbon nanospheres are uniformly sized at around 350 nm, and exist in regularly arranged close-packed arrays of considerable extent. Comparing Figure 1b with Figure 1a, it is obvious that this morphology is inherited from the PRNS precursor. This can be attributed to the thermoset nature of the phenol precursor and the rigid non-graphitizing carbon structure that is formed once it is carbonized.[31] Shrinkage of around 20% in the nanosphere diameter occurs as the PRNS is converted to NCNS, which equates to around 50% in volumetric terms. In contrast, the weight loss that occurs is over 90 %. This implies abundant porosity within the NCNS.

The nitrogen adsorption/desorption isotherms shown in Figure 1d reveal the pore structure of the NCNS. The isotherm exhibits Type Ib features,[32] indicating a highly microporous structure within

the nanospheres. There is an initial rapid uptake of N_2 to a plateau of 900 mL(STP) g^{-1} *via* an open knee that ends at relative pressure (p/p^o) around 0.2. A second rapid uptake to a plateau of around 1400 mL(STP) g^{-1} occurs just prior to saturation. A close-up of this region (Figure 1d upper inset) reveals saturation occurs prior to $p/p^o = 1$ and hysteresis between the adsorption and desorption isotherms, suggesting that this second rapid uptake of N_2 is due to capillary condensation within the uniform mesoporosity between the close-packed nanospheres.

The pore size distribution obtained using quenched solid density functional theory (QSDFT)[33] is shown in the lower inset of Figure 1d. This indicates that the porosity within the carbon nanospheres is dominated preferentially by micropores (*i.e.* less than 2nm in width). One group is centered around 1 nm with a narrow distribution and another has a broad span from 1nm to 2.5 nm, which is reflected in the open knee of the nitrogen isotherm. The specific micropore volume is evaluated using the Dubinin-Radushkevich equation to be 1.0 cm^3 g^{-1} out of a total specific pore volume of 2.3 cm^3 g^{-1}. The difference between these two volumes is sufficient to accommodate the Li-S volume expansion during discharge,[34] thus helps to avoid physical damage to the cathode.

The chemistry of the carbon material was characterized using X-ray photoelectron spectroscopy (XPS). As the survey scan in Figure 1e indicates, the material is composed of C (94 wt%), O (1 wt%) and N (5 wt%). The high resolution N1s scan, which is shown along with its deconvolution inset to Figure 1e, reveals a pyridinic N (398.4 eV), pyrrolic N (400.5 eV), and quaternary N (402.5 eV) atomic ratio of 3:4:3. The pyridinic and pyrrolic N, which are known to be good for immobilizing LiPS compared to pristine carbon surfaces,[35, 36] together constitute 70% of the total nitrogen content. This is illustrated here by the results of a simple solution phase adsorption test,[15, 37] Figure 1f. This figure shows the colour change in a 20 mL 4 mM Li_2S_6 solution after 50 mg of NCNS and Super P carbon black, a reference carbon used by many in the field,[10, 15, 37, 38] were

added. The change in solution colour is marked for the NCNS, whilst little change can be observed for Super P.

By determining the concentrations of Li_2S_6 after the adsorption test using UV-Vis spectrophotometry (details in Supporting Information (SI): **Figure S1**), the Li_2S_6 uptake on the NCNS is estimated to be better than 0.25 g/g, 20 times that of Super P. Interestingly, this level of LiPS adsorbability is also greater than that observed for N-doped mesoporous carbons,[15, 37] suggesting that the abundant microporosity and high surface area of the NCNS is also playing a role in the adsorption of the Li_2S_6.

The NCNS-S70 cathode material was subjected to X-ray diffraction (XRD) and thermogravimetric analysis (TGA). The results suggest that sulfur is well-confined within the micropores of the carbon as an amorphous phase (SI: **Figure S2** and **Figure S3**). High resolution transmission electron microscopy (HRTEM) images (**Figure 2a-c**) and the diffuse rings in the selected area electron diffraction (SAED) pattern (**Figure 2a inset**) for the NCNS-S70 material indicate a non-graphitizing porous carbon microstructure[39] and, in line with the XRD and TGA results, an absence of crystalline sulfur.

Figure 2b reveals one example of multiple interconnections observed between adjacent nanospheres. A close-up of one of these interconnections in Figure 2c indicates that these interconnections have the same carbon microstructure as observed on the edge of the nanospheres (Figure 2a). This suggests that the interconnections are formed during the carbonization process together with the carbon nanospheres. These carbonaceous connections will have helped in maintaining the close-packed cluster morphology in the processing of the PRNS to form the NCNS, and should also aid electrical conductivity between the nanospheres[15] and, thus, throughout the fabricated cathode.

The scanning transmission electron microscopy (STEM) high-angle annular dark-field (HAADF) image in Figure 2d suggests a uniform microstructure throughout the nanospheres, whilst Figures 2e-g are also indicative of homogeneous distributions of C, N and S in the nanospheres. The homogeneous sulfur distribution maximizes the access of sulfur to the large, N-functionalized pore surface of the NCNS. The uniformly distributed sulfur confined within the NCNS porous structure also explains the TGA results (SI: Figure S3), where sulfur loss was found to take place at substantially higher temperatures and at a slower rate compared with pristine sulfur powder.

2.2. Cathode morphology and electrochemical performance

The cathodes were formed by slurry coating the cathode material onto a carbon-coated Al current collectors with carbon black and PVDF binders. Apart from the cathodes containing 5 mg cm^{-2} sulfur, thinner cathodes containing 2 mg cm^{-2} sulfur were also made and tested here for comparison. The structure of the thicker cathode was characterized using SEM, **Figure 3**a-c. Figure 3a shows the top view of the fabricated cathode surface at low magnification. The cathode surface appears to be densely packed and crack-free. The higher resolution image in Figure 3b shows that the nanospheres exist in close-packed clusters up to a few micrometres in extent. The continued existence of these close-packed clusters is evident despite the compositing with sulfur and subsequent coating onto the current collector. This indicates the carbonaceous connections between the nanospheres as shown in Figure 2b are very robust indeed. This is clearly inherited from the NCNS (Figure 1b-c) morphology. Such clustering helps to minimize shrinkage during drying of the slurry, which in turn helps to avoid cracking in the cathode.

To evaluate the cathode structure through its depth, the 5 mg cm^{-2} cathode was embedded in epoxy resin and sectioned for cross-sectional SEM imaging. As seen in Figure 3c, the cathode is essentially homogeneous crack-free from the current collector at the bottom through to its upper

surface. A smooth interface can be seen between the cathode material and current collector, which ensures good electrical conductivity into the latter. The cathode coating thickness is around 50 µm.

A Li-S cell containing the 5 mg cm^{-2} cathode was subject to cyclic voltammetry (CV) at a scan rate of 0.1 mV s^{-1} between 3.0 V and 1.5 V. The results, which are shown in Figure 3d, clearly indicate two redox pairs. The first, which occurs at around 2.2 V, can be attributed to the reduction of sulfur to soluble long chain LiPS (Li_2S_x, $4 < x < 8$), whilst the second at around 2.0 V is due to the further reduction of these LiPS to short chain insoluble sulfides (Li_2S_x, $1 < x < 4$).[40] The second of these cathodic peaks up-shifts over the first 5 scans, indicating that the cathode undergoes an activation process in the initial cycles. A broad anodic peak spanning between 2.1V to 2.8V exists in all the spectra. It can be seen that this peak is in fact formed of two closely located anodic peaks that represent the reverse of the cathodic counterparts[40] and can be attributed to the continuous micropore-confined oxidization of Li_2S to LiPS and, finally, sulfur. Little difference can be found between the spectra of scan 5 and scan 10, indicating the cathode had stabilized after the first 5 scans.

Electrochemical impedance spectroscopy (EIS) results for a cell containing the 5 mg cm^{-2} cathode at the charged-state are shown in Figure 3e. The spectrum of the virgin cell is dominated by a large depressed semi-circle. This, however, changed significantly over the first 25 charge-discharge cycles (C25) before stabilizing (*c.f.* C100 spectrum). Two depressed semi-circles are evident in the high frequency region of the C25 and C100 spectra, which can be attributed to electrode-electrolyte charge transfer resistance (R_{ct}, higher frequency) and interphase resistance between the conducting carbon matrix and sulfur (R_{int}, lower frequency), respectively.[16, 41]

To enable quantitative analysis, an equivalent circuit model[41] is employed to fit the experimental spectra (details in SI: **Figure S4** and **Table S1**). The impedance of the uncycled cell is found to be

caused predominately by a large R_{ct} of 140.7 Ω. This is related to the insufficient electrolyte wetting of the cathode before cycling[41, 42]. After 25 and 100 cycles of charge-discharge, R_{int} decreased to 35.8 Ω and 33.2 Ω respectively. This is consistent with the gradual change of the CV profiles with the increasing number of scans (Figure 3d). R_{ct} remains low over the 100 cycles, the values being 8.0 Ω, 12.3 Ω and 14.4 Ω for the uncycled, 25 and 100 cycles, respectively. This stable low impedance originates from the highly conductive carbon matrix formed by the NCNS, the sufficient ion-diffusion channels between the close-packed nanospheres and the good fixation of sulfur within the carbon porous structure.

Galvanostatic charge-discharge curves collected at three different C rates (0.05C, 0.2C and 0.5C, where 1C = 1672 mA g^{-1} of sulfur) on cells fabricated from the 5 mg cm^{-2} and thinner 2 mg cm^{-2} cathodes are shown in Figure 3f. The thinner cathodes were tested to evaluate the effect of cathode thickness on performance. Owing to the above mentioned cathode activation over the initial cycles, charge-discharge curves from the 25^{th} cycle are compared. The C rate appears to have little impact on the overall shape of both the charge and discharge curves. The charge curves start with a small over-potential of around 2.25 V before they go on to steadily increase with specific capacity from 2.2 V to 2.4 V. The discharge curves exhibit the two typical discharge plateaus. In agreement with the CV profiles, the first at around 2.3 V correlates to the conversion of sulfur to long chain LiPS, whilst the second from 2.1 to 2 V is due to the continued discharge where the long chain LiPS are converted to Li_2S.

A high 1395 mAh g^{-1} discharge specific capacity was achieved on the thin cathode at 0.05C to a cut-off potential of 1.7 V. Severe $LiNO_3$ (electrolyte additive, see Experimental Section) reduction[43] was observed below 1.7 V at 0.05C for the thin cathode whilst the value is found to be 1.5 V and lower in all the other situations considered here. At the higher charge/discharge rates

of 0.2C and 0.5C, the specific capacity of the thin cathode was found to be 1160 mAh g^{-1} and 934 mAh g^{-1}, respectively (i.e. 83% and 67% of the 0.05C value). The 5 mg cm^{-2} S cathode yielded discharge capacities of 1284, 1065 and 874 mAh g^{-1} for 0.05C, 0.2C and 0.5C respectively, which are over 90% of those achieved for the thinner cathode considered here. Considering the cathode thickness shown in Figure 3c (50 µm of the cathode coating plus 18 µm of the current collector), the volumetric capacity of the thicker cathode is calculated to be 917, 760 and 624 mAh cm^{-3} for 0.05C, 0.2C and 0.5C, respectively, amongst the highest reported to date. Around 0.1 V polarization is visible at 0.5C on the discharge curve of the thick cathode. This indicates that ion diffusion is a limiting factor at 0.5C, and the cells were not tested at C rates higher than this.

Cells containing the 5 mg cm^{-2} cathodes were subjected to long-term cycling at 0.5C and 0.2C to evaluate cell stability. At the higher rate, 500 charge-discharge cycles were performed (**Figure 4**a), whilst 200 cycles were performed at 0.2C (Figure 4b). At 0.5C, the cell presents with an initial discharge capacity of 1196 mAh g^{-1}. This capacity drops over the first 25 cycles, however, to 874 mAh g^{-1} whilst the Coulombic efficiency drops from 108% to 95% before gradually stabilizing at around 97%. The above-100% Coulombic efficiency in the first few cycles indicates mild dissolution of sulfur into the electrolyte, which becomes irreversible in the following cycles.

Figure 4c shows the change of the 0.5C Galvanostatic charge-discharge curves over the 500 cycles. The change in the curve shape over the first 25 cycles arises from a gradual reduction in polarization of the second discharge plateau. From cycle 25 onwards, the dual-plateau discharge curve shape is maintained, with the second plateau stabilizing at around 2.0 V. The specific capacity at cycle 500 is 672 mAh g^{-1}, which is 56% of the initial capacity; this corresponds to an average capacity fading rate of 0.1% per cycle.

At 0.2C, the cell delivers a higher initial specific capacity of 1309 mAh g^{-1}. The cell activation process observed at 0.5C was also found for the slower rate up to around cycle 15. After 200 cycles, the capacity dropped to 797 mAh g^{-1}. It is clear that over the first 200 cycles, the cathode areal capacity remains above 4 mAh cm^{-2}, a typical value for Li-ion batteries.[24]

2.3 Cathode volumetric capacity and 'cathode region' gravimetric capacity

The 5 mg cm^{-2} sulfur loaded cathode based on the NCNS is compared here with other recently reported results[24-29, 34, 44-49] in cathode volumetric capacity and what we term *'cathode region' gravimetric capacity*. The values are evaluated using the 25th cycle data at 0.2C, which is widely available. Cathode volumetric capacity, C_V^{cat}, is calculated using

$$C_V^{cat} = \frac{C_S \times A_S}{d_{cat}} \quad (1)$$

where C_S is the specific sulfur capacity, A_S the areal sulfur loading, and d_{cat} the thickness of the cathode (including the current collector). To reflect the influence of cathode structure on the required electrolyte fraction and overall gravimetric capacity, 'cathode region' gravimetric capacity, C_G^{cat}, as per the following is considered

$$C_G^{cat} = \frac{C_S \times A_S}{\frac{A_S}{f_S} + 0.5 \times C_S \times f_{elec} \times \rho_{elec}} \quad (2)$$

where f_S is the fraction of sulfur in the cathode solid phase (w/w, including current collector), f_{elec} the electrolyte fraction (µL mg^{-1} of sulfur), and ρ_{elec}. the electrolyte density (1mg μL^{-1} [20]). It is assumed that 50% of the total electrolyte mass contributes to the mass of the 'cathode region'.

As **Figure 5**a shows the cell based on the 5 mg cm^{-2} sulfur NCNS cathode compares very favorably with other state-of-the-art systems (calculated values are shown in SI: **Table S2**). Our cathode is in the top three, with the other two (from references 22 and 23) having slightly higher volumetric capacity but less 'cathode region' gravimetric capacity or *vice versa*. The batteries falling within

the broken red circle in Figure 5a are projected to be competitive with state-of-the-art Panasonic NCR18650B Li-ion battery[20] in terms of gravimetric energy density (i.e. 200 Wh kg^{-1}, details of calculation in SI). In particular, the battery considered here together with the cells demonstrated by Chung *et al.*[25] are competitive in volumetric energy density (i.e. 600 Wh L^{-1}) as well.

Further comparison in Figure 5b indicates this work to be amongst the best in the field in cathode sulfur density (gram of sulfur per cm^3 of cathode volume, including current collector). This in turn can lead to larger cathode volumetric capacity. An overall increasing trend of 'cathode region' gravimetric capacity against cathode sulfur density is also apparent from these results. It is generally believed that lower cathode sulfur density helps to improve sulfur-carbon contact for better sulfur utilization and higher specific capacity. However, the analysis here suggests that the electrolyte used to fill the large fraction of macropores in the low sulfur density cathodes acts to reduce the overall gravimetric capacity. The electrolyte fraction required for the thick NCNS cathodes here is 6 µL mg^{-1}, within the range required for thin low areal sulfur loading cathodes.[20, 22] In comparison, substantially higher electrolyte fractions (29 µL mg^{-1} [27] and 14 µL mg^{-1} [28, 29]) were used for those that appear to have the lowest 'cathode region' gravimetric capacities (See SI: Table S2 for details.). With cathode sulfur density greater than 0.6 g cm^{-3}, the cathode reported here demonstrates the possibility to achieve high gravimetric and volumetric capacities *via* micro-scale material design plus mesoscale cathode structuring.

3. Conclusion

5 mg cm^{-2} high sulfur loading cathodes were fabricated using a sulfur-host composed of interconnected close-packed monodisperse highly porous nitrogen-doped carbon nanospheres. The micro- and meso-structure of the carbon material enables high sulfur utilization and stable long-life cycling performance. The abundant micropores with large specific area N-doped surfaces

provide excellent LiPS adsorbability and, hence, immobilization of sulfur. The high pore volume of the carbon nanospheres facilitates high sulfur loading (70 wt%) whilst the mesoporosity in the close-packed clusters between individual nanospheres ensures long-life cycling by avoiding damage caused by the volume expansion of the Li_2S during discharge. The interconnected and close-packed structure of the nanospheres also offers good electrical conductivity, sufficient ion-diffusion channels and low electrochemical impedance. These characteristics together provide a comprehensive solution to yield high sulfur specific capacities and high cathode volumetric capacities. The unique structure of the carbon also enables the formation of thick crack-free cathodes with a compact macro-structure. This leads to a high cathode sulfur density of 0.6 g cm^{-3}, a low electrolyte content and, thus, high 'cathode region' and overall gravimetric capacities. The excellent performance combined with the facile synthesis and fabrication route makes the cathode material competitive for industrial scale-up.

4. Experimental Section

Preparation of NCNS and NCNS-S70: PRNS was synthesized following Zhao *et al*.[30] The resulting PRNS dispersion was washed with ethanol three times and centrifuged at 10000 rpm for 30 min to collect the solid PRNS. After drying at 90 °C overnight, 5 g of the PRNS was transferred to an alumina boat that was then placed in the centre of a tube furnace for carbonization, activation and nitrogenation. Carbonization was carried out under 500 mL min^{-1} flow of Ar. The furnace temperature was ramped to 900 °C at 1 °C min^{-1} and held for two hours. During the ramping, the temperature was paused for 2 hours at 210 °C and 650 °C respectively. The flowing gas was shifted to 1000 mL min^{-1} CO_2 at the end of the carbonization and the temperature was maintained at 900 °C for a further 15 hours during which the carbonized product was activated. At the end of the activation the temperature was decreased from 900 °C to 600 °C at 3 °C min^{-1} whilst the tube furnace was purged with N_2 at 1000mL min^{-1}. 200mL min^{-1} ammonia was introduced when the furnace reached 600 °C and the temperature was maintained for 6 hours to allow nitrogenation. 0.45 g NCNS was collected as the final product. To synthesize NCNS-S70, 0.3 g of NCNS was ground with 0.75 g sulfur powder (99.9%) for 20 min before being heated to 155 °C at 1 °C min^{-1}

and held for 24 hours. Heating was done in a small sealed tube furnace filled with N_2 at a pressure of 0.8 bar.

Material Characterization: Scanning electron microscopy (SEM) was performed on a JEOL JSM-7800F microscope operating at 5 kV. A fabricated cathode was embedded in epoxy resin and cut with a sharp razor blade for cross-sectional imaging. Scanning/Transmission electron microscopy (S/TEM) was performed on a FEI Tecnai F20 field emission gun microscope operating at 200 kV. The microscope is equipped with a Gatan Multiscan CCD Camera, a Fischione high-angle annular dark-field (HAADF) detector and an Oxford Instruments X-Max 80 mm^2 window-less energy-dispersive spectrometer (EDS). N_2 adsorption and desorption was performed using a Quadrasorb-Kr/MP apparatus from Quantachrome Corp. Samples were degassed at 250 ºC for 8 hours under high-vacuum (10^{-4} Pa) before the isotherms were measured. Specific surface area was calculated using the Brunauer–Emmett–Teller (BET) model following the recommendation for microporous materials.[50] Specific pore volume was calculated using the Dubinin-Radushkevich equation. Pore size distribution was calculated using the quenched solid density functional theory (QSDFT) models.[33] X-ray photoelectron Spectroscopy (XPS) was performed on a Thermo Scientific K-Alpha spectrometer with a monochromated Al kα x-ray source. X-ray diffraction was performed on a Bruker D8 Advance Cu kα diffractometer. Diffraction patterns were collected from 2θ of 10° to 90° at around 1° min^{-1} with a step size of 0.016°. Thermogravimetric analysis (TGA) was performed on a TA Instruments Q600 analyzer. Analysis was done with around 10 mg of sample under 100 mL min^{-1} flow of N_2 and 10 °C min^{-1} heating rate. Solution phase Li_2S_6 adsorption tests were performed following reported procedures (details in SI).[15, 37]

Electrochemical Measurements: Cathodes with 2 mg cm^{-2} S and 5 mg cm^{-2} S were prepared by the conventional slurry coating method. Briefly, NCNS-S70 (85 wt%), Super P (7.5 wt%) and polyvinylidene fluoride (7.5 wt%) were mixed and stirred in N-methyl-2-pyrrolidinone (NMP) overnight to form a homogeneous slurry. The slurry was then blade coated onto a carbon-coated Al foil (MTI, 18 µm thick) and vacuum dried at 65 °C for 24 hours. Cathode mass was measured using a laboratory analytical balance (FISHER SCITIFIC). Cathode thickness was measured using a digital micrometer (MITUTOYO 395). The cathode coating thickness was around 18 µm and 50 µm for the thin and thick cathodes, respectively. CR2032-type test cells were assembled in an Ar-filled glove box (MBRAUN LABstar). Lithium foils (99.9%, 750 µm thick) punched to 16 mm diameter discs were used as anodes. The prepared cathodes were punched into 12 mm diameter

discs. Celgard 2325 membranes were used as separators. The electrolyte was LiTFSI (1M) plus $LiNO_3$ (1 wt%) dissolved in 1:1 (v/v) mixture of 1,3-dioxolane (99.5% anhydrous) and 1,2-dimethoxyethane (99.9%, anhydrous) and the electrolyte to sulfur ratio was 6 µL mg^{-1} for a whole cell. Cyclic voltammetry was performed on a METROHM µAUTOLAB potentiostat between 1.5 V and 3.0 V at a scan rate of 0.1 mV/s. Electrochemical impedance spectroscopy (EIS) was performed on a potentiostat/galvanostat (Princeton Applied Research 263A) coupled with a frequency response analyzer (SOLARTRON 1250). The frequency range was 100 kHz to 0.1 Hz and the perturbation amplitude was 5 mV. The equivalent circuit model proposed by Deng *et al.*[41] was used to analyze the collected spectra. Galvanostatic charge-discharge measurements were performed on a NEWARE BTS9000 battery testing system. C rates were determined on the cells' sulfur contents, where 1 C = 1672 mA per g of sulfur.

Supporting Information

Supporting Information is available from the Wiley Online Library or from the author.

Acknowledgements

CH acknowledges a Postdoctoral Fellowship provided by Loughborough University. Dr. Zhaoxia Zhou at Loughborough Materials Characterization Centre, Loughborough University is gratefully acknowledged for assistance with the TEM work. QC gratefully acknowledges the support by the EPSRC program EP/M027066/1

Received: ((will be filled in by the editorial staff))
Revised: ((will be filled in by the editorial staff))
Published online: ((will be filled in by the editorial staff))

References

[1] Y. Yang, G. Zheng, Y. Cui, *Chem. Soc. Rev.* **2013**, 42, 3018.

[2] L. F. Nazar, M. Cuisinier, Q. Pang, *MRS Bulletin* **2014**, 39, 436.

[3] R. Xu, I. Belharouak, J. C. M. Li, X. Zhang, I. Bloom, J. Bareño, *Adv. Energy Mater.* **2013**, 3, 833.

[4] Y. Diao, K. Xie, S. Xiong, X. Hong, *J. Electrochem. Soc.* **2012**, 159, A421.

[5] Y. V. Mikhaylik, J. R. Akridge, *J. Electrochem. Soc.* **2004**, 151, A1969.

[6] H. Yamin, A. Gorenshtein, J. Penciner, Y. Sternberg, E. Peled, *J. Electrochem. Soc.* **1988**, 135, 1045.

[7] S.-E. Cheon, K.-S. Ko, J.-H. Cho, S.-W. Kim, E.-Y. Chin, H.-T. Kim, *J. Electrochem. Soc.* **2003**, 150, A800.

[8] X. Ji, L. F. Nazar, *J. Mater. Chem.* **2010**, 20, 9821.

[9] X. Ji, K. T. Lee, L. F. Nazar, *Nat. Mater.* **2009**, 8, 500.

[10] Y.-J. Li, J.-M. Fan, M.-S. Zheng, Q.-F. Dong, *Energy Environ. Sci.* **2016**, 9, 1998.

[11] Q. Pang, J. Tang, H. Huang, X. Liang, C. Hart, K. C. Tam, L. F. Nazar, *Adv. Mater.* **2015**, 27, 6021.

[12] J. Schuster, G. He, B. Mandlmeier, T. Yim, K. T. Lee, T. Bein, L. F. Nazar, *Angew. Chem., Int. Ed. Engl.* **2012**, 51, 3591.

[13] G. He, S. Evers, X. Liang, M. Cuisinier, A. Garsuch, L. F. Nazar, *ACS Nano* **2013**, 7, 10920.

[14] S. Niu, G. Zhou, W. Lv, H. Shi, C. Luo, Y. He, B. Li, Q.-H. Yang, F. Kang, *Carbon* **2016**, 109, 1.

[15] Q. Sun, B. He, X. Q. Zhang, A. H. Lu, *ACS Nano* **2015**, 9, 8504.

[16] B. Zhang, X. Qin, G. R. Li, X. P. Gao, *Energy Environ. Sci.* **2010**, 3, 1531.

[17] Z. Li, Y. Jiang, L. Yuan, Z. Yi, C. Wu, Y. Liu, P. Strasser, Y. Huang, *ACS Nano* **2014**, 8, 9295.

[18] M. Q. Zhao, M. Sedran, Z. Ling, M. R. Lukatskaya, O. Mashtalir, M. Ghidiu, B. Dyatkin, D. J. Tallman, T. Djenizian, M. W. Barsoum, Y. Gogotsi, *Angew. Chem., Int. Ed. Engl.* **2015**, 54, 4810.

[19] H. Chen, C. Wang, W. Dong, W. Lu, Z. Du, L. Chen, *Nano Lett.* **2015**, 15, 798.

[20] M. Hagen, D. Hanselmann, K. Ahlbrecht, R. Maça, D. Gerber, J. Tübke, *Adv. Energy Mater.* **2015**, 5, 1401686.

[21] R. Fang, S. Zhao, Z. Sun, D.-W. Wang, H.-M. Cheng, F. Li, *Adv. Mater.* **2017**, 1606823.

[22] M. A. Pope, I. A. Aksay, *Adv. Energy Mater.* **2015**, 5, 1500124.

[23] D. Lv, J. Zheng, Q. Li, X. Xie, S. Ferrara, Z. Nie, L. B. Mehdi, N. D. Browning, J.-G. Zhang, G. L. Graff, J. Liu, J. Xiao, *Adv. Energy Mater.* **2015**, 5, 1402290.

[24] R. Fang, S. Zhao, P. Hou, M. Cheng, S. Wang, H.-M. Cheng, C. Liu, F. Li, *Adv. Mater.* **2016**, 28, 3374.

[25] S.-H. Chung, C.-H. Chang, A. Manthiram, *ACS Nano* **2016**, 10, 10462.

[26] S.-H. Chung, C.-H. Chang, A. Manthiram, *Energy Environ. Sci.* **2016**, 9, 3188.

[27] G. Hu, C. Xu, Z. Sun, S. Wang, H.-M. Cheng, F. Li, W. Ren, *Adv. Mater.* **2016**, 28, 1603.

[28] L. Qie, C. Zu, A. Manthiram, *Adv. Energy Mater.* **2016**, 6, 1502459.

[29] H. Xu, L. Qie, A. Manthiram, *Nano Energy* **2016**, 26, 224.

[30] J. Zhao, W. Niu, L. Zhang, H. Cai, M. Han, Y. Yuan, S. Majeed, S. Anjum, G. Xu, *Macromolecules* **2013**, 46, 140.

[31] H. Teng, S.-C. Wang, *Carbon* **2000**, 38, 817.

[32] M. Thommes, K. Kaneko, V. Neimark Alexander, P. Olivier James, F. Rodriguez-Reinoso, J. Rouquerol, K. S. W. Sing, *Pure Appl. Chem.* **2015**, 87, 1051.

[33] A. V. Neimark, Y. Lin, P. I. Ravikovitch, M. Thommes, *Carbon* **2009**, 47, 1617.

[34] R. Fang, S. Zhao, S. Pei, X. Qian, P.-X. Hou, H.-M. Cheng, C. Liu, F. Li, *ACS Nano* **2016**, 10, 8676.

[35] J.-J. Chen, R.-M. Yuan, J.-M. Feng, Q. Zhang, J.-X. Huang, G. Fu, M.-S. Zheng, B. Ren, Q.-F. Dong, *Chem. Mater.* **2015**, 27, 2048.

[36] Y. Qiu, W. Li, W. Zhao, G. Li, Y. Hou, M. Liu, L. Zhou, F. Ye, H. Li, Z. Wei, S. Yang, W. Duan, Y. Ye, J. Guo, Y. Zhang, *Nano Lett.* **2014**, 14, 4821.

[37] J. Song, M. L. Gordin, T. Xu, S. Chen, Z. Yu, H. Sohn, J. Lu, Y. Ren, Y. Duan, D. Wang, *Angew. Chem., Int. Ed. Engl.* **2015**, 54, 4325.

[38] C. J. Hart, M. Cuisinier, X. Liang, D. Kundu, A. Garsuch, L. F. Nazar, *Chem Commun* **2015**, 51, 2308.

[39] Z.-l. Zhang, R. Brydson, Z. Aslam, S. Reddy, A. Brown, A. Westwood, B. Rand, *Carbon* **2011**, 49, 5049.

[40] Y. X. Yin, S. Xin, Y. G. Guo, L. J. Wan, *Angew. Chem., Int. Ed.* **2013**, 52, 13186.

[41] Z. Deng, Z. Zhang, Y. Lai, J. Liu, J. Li, Y. Liu, *J. Electrochem. Soc.* **2013**, 160, A553.

[42] C. P. Yang, Y. X. Yin, H. Ye, K. C. Jiang, J. Zhang, Y. G. Guo, *ACS Appl. Mater. Interfaces* **2014**, 6, 8789.

[43] S. S. Zhang, *J. Electrochem. Soc.* **2012**, 159, A920.

[44] G. Ai, Y. Dai, W. Mao, H. Zhao, Y. Fu, X. Song, Y. En, V. S. Battaglia, V. Srinivasan, G. Liu, *Nano Lett.* **2016**, 16, 5365.

[45] Q. Pang, L. F. Nazar, *ACS Nano* **2016**, 10, 4111.

[46] H.-J. Peng, W.-T. Xu, L. Zhu, D.-W. Wang, J.-Q. Huang, X.-B. Cheng, Z. Yuan, F. Wei, Q. Zhang, *Adv. Funct. Mater.* **2016**, 26, 6351.

[47] Z. Yuan, H.-J. Peng, J.-Q. Huang, X.-Y. Liu, D.-W. Wang, X.-B. Cheng, Q. Zhang, *Adv. Funct. Mater.* **2014**, 24, 6105.

[48] L. Qie, A. Manthiram, *Adv. Mater.* **2015**, 27, 1694.

[49] Q. Pang, X. Liang, C. Y. Kwok, J. Kulisch, L. F. Nazar, *Adv. Energy Mater.* **2017**, 7, 1601630.

[50] J. Rouquerol, P. Llewellyn, F. Rouquerol, in *Studies in Surface Science and Catalysis*, Vol. 160 (Eds: P. L. Llewellyn, F. Rodriquez-Reinoso, J. Rouqerol, N. Seaton), Elsevier, Amsterdam and Oxford **2007**, pp 49-56.

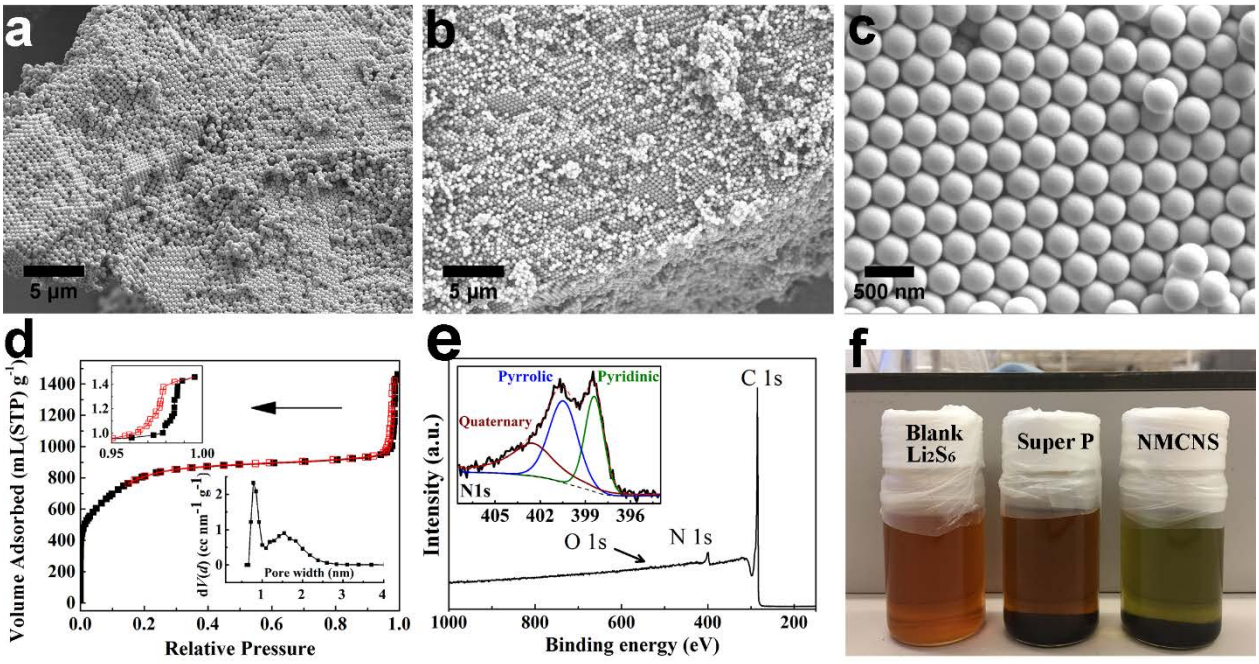

Figure 1. Structural characterization of the NCNS used as the basis for the Li-S cathode: (a) SEM image of the PRNS precursor clearly showing the polymeric nanospheres in extended close packed structures; (b) SEM image of a cluster of the NCNS obtained from the PRNS showing that the close packing in the precursor is retained to a significant extent; (c) high magnification SEM image of the close-packed NCNS arrays; (d) Nitrogen adsorption (black) and desorption (red) isotherms and the derived pore size distribution; (e) XPS full survey and high-resolution N1s scan, which is deconvoluted into contributions from pyridinic N (398.4 eV), pyrrolic N (400.5 eV), and quaternary N (402.5 eV); and (f) Adsorption of Li_2S_6 by the NCNS and Super P.

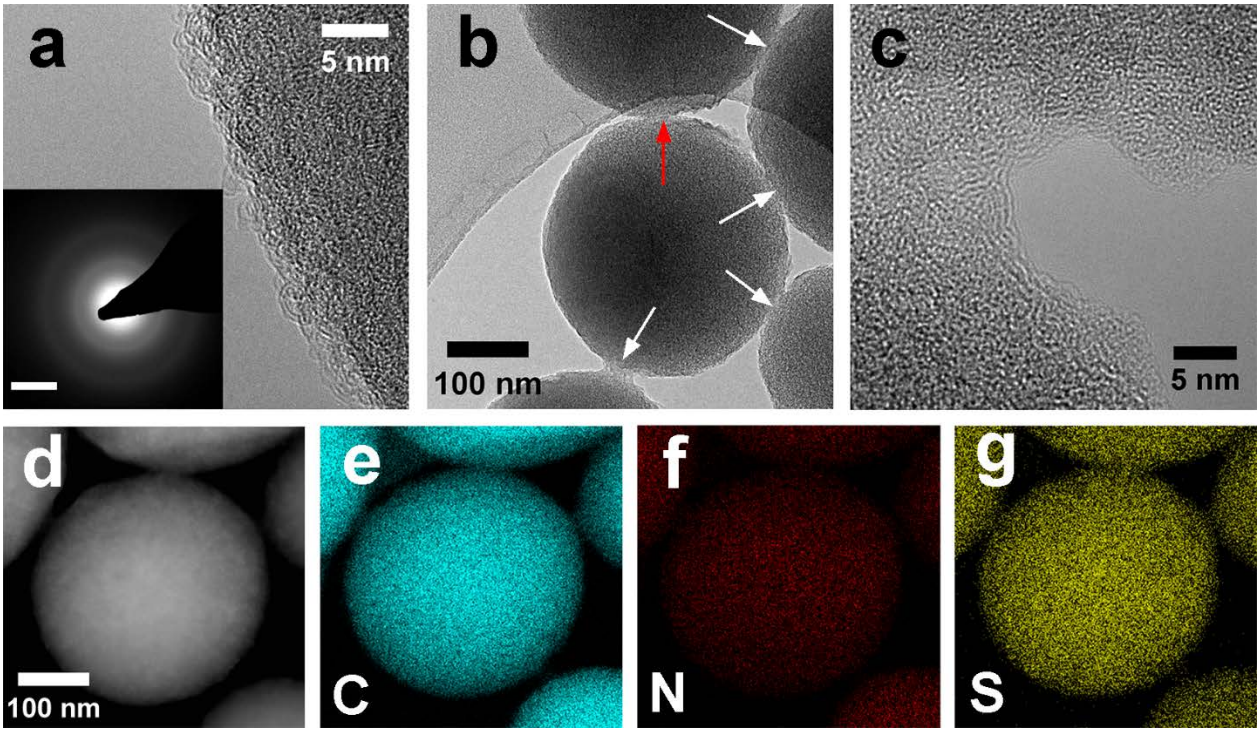

Figure 2. Microstructure of the NCNS-S70 as characterized by S/TEM: (a) HRTEM image of the microstructure at the edge of a nanosphere with the SAED pattern from one of the nanospheres shown inset (scale bar is 5 nm^{-1}); (b) HRTEM image of the interconnections between nanospheres (indicated by arrows); (c) a close-up HRTEM image of one interconnection (red arrow); (d) HAADF image of a nanosphere; (e) corresponding elemental C mapping in the nanosphere; (f) elemental N mapping; (g) elemental S mapping. Plates (d) to (g) share the scale bar in (d).

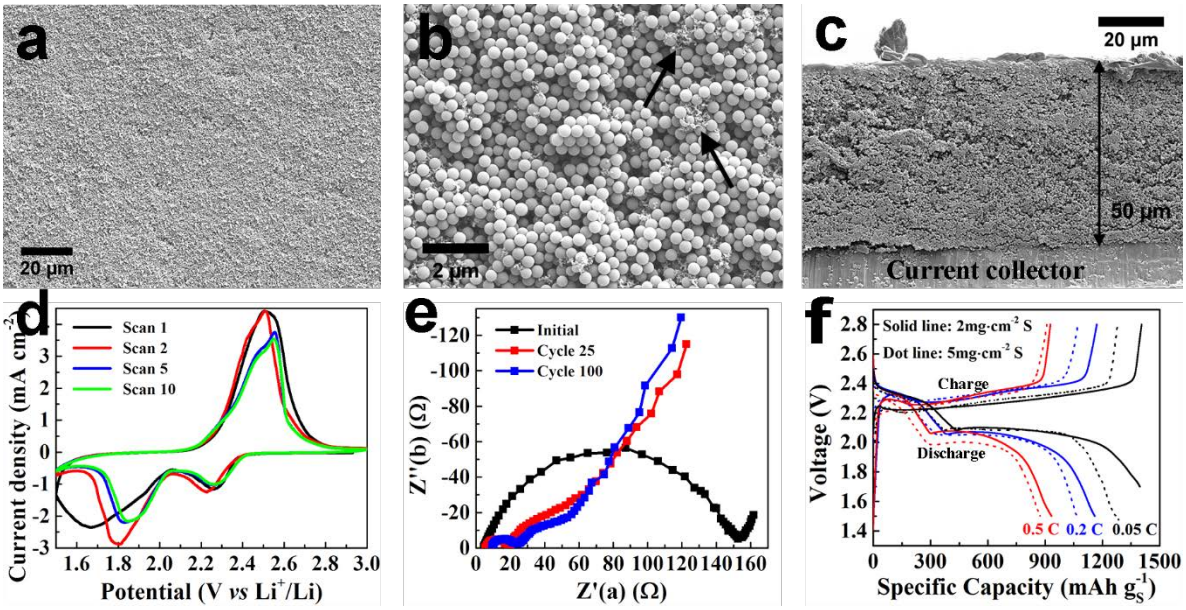

Figure 3. Structure and electrochemical properties of the cathode: (a) low magnification SEM image of the top surface of the 5mg cm^{-2} S cathode; (b) high magnification SEM image of the top surface of the 5mg cm^{-2} S cathode (arrows indicate the conductive carbon black binder); (c) low resolution SEM image of the cross-section of the 5mg cm^{-2} S cathode; (d) cyclic voltammetry profiles of the Li-S cell based on the 5mg cm^{-2} S cathode; (e) ESI Nyquist plots of the Li-S cell based on the 5mg cm^{-2} S cathode; and (f) charge/discharge profiles of the Li-S cell based on the 2mg cm^{-2} S and 5mg cm^{-2} S cathodes at different C rates.

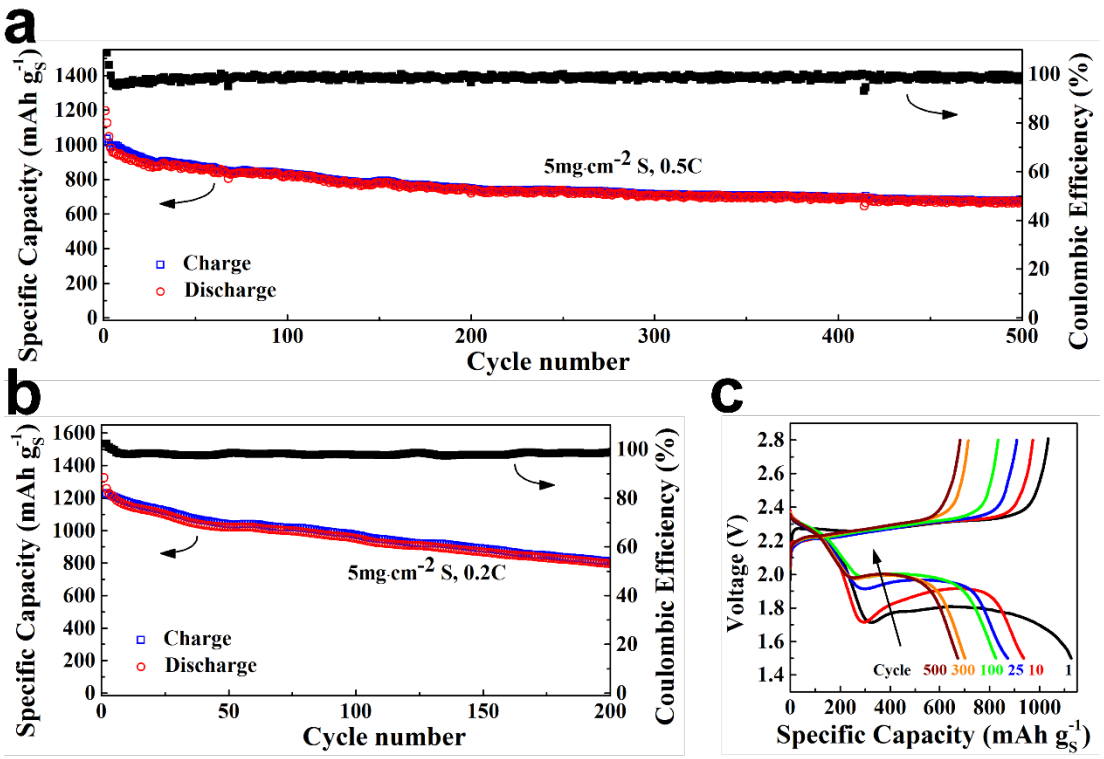

Figure 4. Long-term cycling performance of Li-S cells made from the thicker (5 mg cm^{-2}) cathodes: (a) Charge/discharge specific capacity and Coulombic efficiency at 0.5C for 500 cycles; (b) Charge/discharge specific capacity and Coulombic efficiency at 0.2C for 200 cycles; and (c) Change of the galvanostatic charge/discharge curves at 0.5C over 500 cycles.

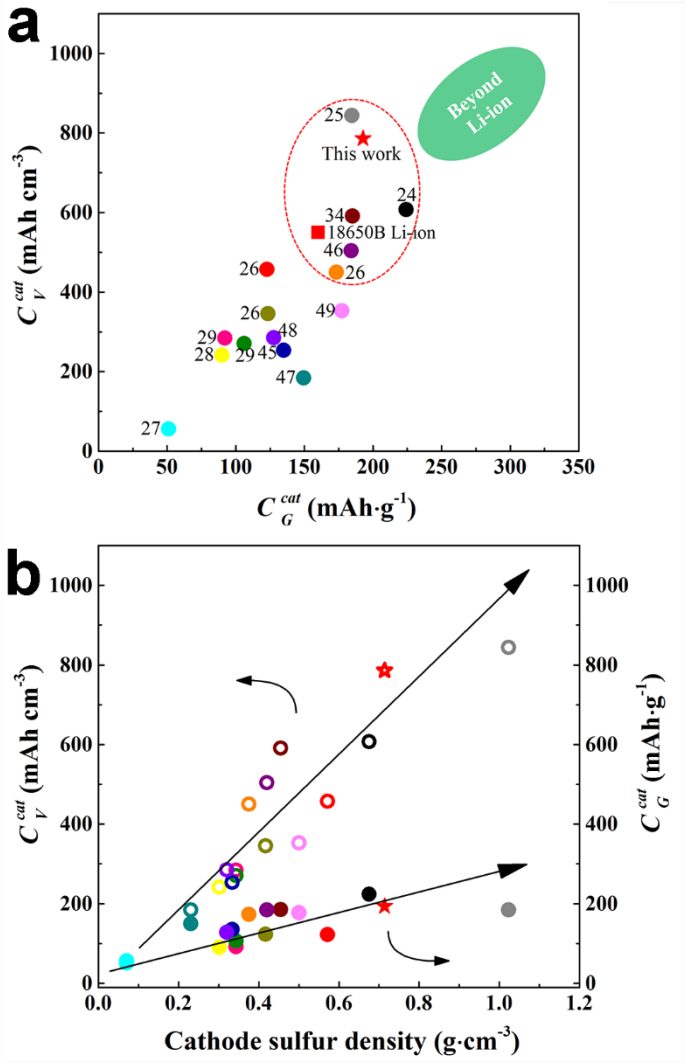

Figure 5. Comparison of the performance of a Li-S cell based on the 5 mg cm^{-2} sulfur loaded cathode reported here (star) against other recently published results (circles with reference numbers): (a) cathode volumetric capacity *vs* cathode gravimetric capacity (the point for the Panasonic NCR18650B Li-ion cell[20] is shown as a red square for reference); and (b) cathode gravimetric (closed symbols) and volumetric capacity (open symbols) *vs* cathode sulfur density. Both plates share the same colour legends.

Li-S battery cathodes providing amongst the best volumetric/gravimetric capacities reported to date are prepared using interconnected close-packed N-doped carbon nanospheres of high surface area and porosity. The novel close-packed meso-structure and N-doped highly porous micro-structure enables simultaneously high sulfur density and utilization, excellent electrochemical impedance, long cycle-life and low electrolyte fraction, which all-together leads to the outstanding volumetric/gravimetric capacities.

Li-S battery, high volumetric capacity, monodisperse, interconnected carbon nanospheres, close-packed

*Cheng Hu, Caroline Kirk, Qiong Cai, Carlos Cuadrado-Collados, Joaquín Silvestre-Albero, Francisco Rodríguez-Reinoso and Mark James Biggs**

A High-Volumetric-Capacity Cathode Based on Interconnected Close-packed N-Doped Porous Carbon Nanospheres for Long-life Lithium–Sulfur Batteries

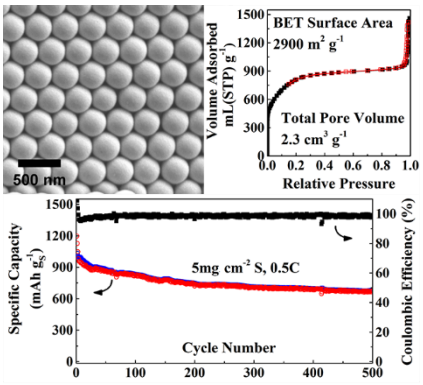

Supporting Information

A High-Volumetric-Capacity Cathode Based on Interconnected Close-packed N-Doped Porous Carbon Nanospheres for Long-life Lithium–Sulfur Batteries

*Cheng Hu, Caroline Kirk, Qiong Cai, Carlos Cuadrado-Collados, Joaquín Silvestre-Albero, Francisco Rodríguez-Reinoso and Mark James Biggs**

Solution Phase Li_2S_6 Adsorption Test

Solution phase Li_2S_6 adsorption tests were performed following reported procedures.[S1, S2] 1.6 g of sulfur powder (99.9%), 0.46 g of Li_2S (99.9%) and 20 mL tetrahydrofuran (THF, 99.5%, anhydrous) were mixed and stirred at 50°C for 48 hours to form a 0.5 M Li_2S_6 solution. The obtained solution was further diluted in THF (99.5%, anhydrous) to 4 mM. 50 mg of adsorbent (NCNS or Super P carbon black) was added to 20 mL of the 4 mM Li_2S_6 solution and stirred at room temperature overnight. The concentration of the resulting adsorption residue solutions was determined by UV-Vis spectrophotometry (Perkin Elmer, Lambda35 spectrophotometer). The resulting solutions from Super P and NCNS were diluted 10 and 5 times respectively and the peak at 420 nm of their UV-Vis spectra were used to quantify the concentrations (Figure S1). Preparation and handling of the Li_2S_6 solutions were carried out in an Ar-filled glove box (MBRAUN LABstar).

Projection of Cell Gravimetric and Volumetric Energy Density

Cell gravimetric energy density is determined by

$$E_G = \frac{C_S \times A_S \times V_a \times (1-f_{pac})}{W_{cat-solid}+W_{elec}+W_{ano}+W_{sep}} = \frac{C_S \times A_S \times V_a \times (1-f_{pac})}{\frac{A_S}{f_S}+A_S \times f_{elec} \times \rho_{elec}+\frac{2 \times C_S \times A_S}{C_{Li}}+W_{sep}} \quad \text{(S1)}$$

where $W_{cat-solid}$, W_{elec}, W_{ano} and W_{sep} are the weight of cathode solid phase (including current collector), electrolyte, anode and separator, respectively. V_a is the average discharge voltage and is used as 2.1 V in this calculation. W_{ano} is projected from the cathode areal capacity by assuming 100% excess in lithium. The specific capacity of lithium C_{Li} used for this calculation is 3860 mAh g^{-1}. W_{sep} is 1 mg cm^{-2} in this calculation. f_{pac} is the weight fraction of projected cell packing and is taken as 10 wt% in this calculation.

Cell volumetric energy density is determined by

$$E_V = \frac{C_S \times A_S \times V_a \times (1-f_{pac})}{d_{cat}+d_{ano}+d_{sep}} = \frac{C_S \times A_S \times V_a \times (1-f_{pac})}{d_{cat}+\frac{2 \times C_S \times A_S}{C_{Li} \times \rho_{Li}}+d_{sep}} \quad \text{(S2)}$$

where d_{cat}, d_{ano} and d_{sep} are the thickness of cathode, anode and separator, respectively. 25 μm is used for d_{sep} in this calculation. ρ_{Li} is the density of lithium and used as 0.53 g cm^{-3}.

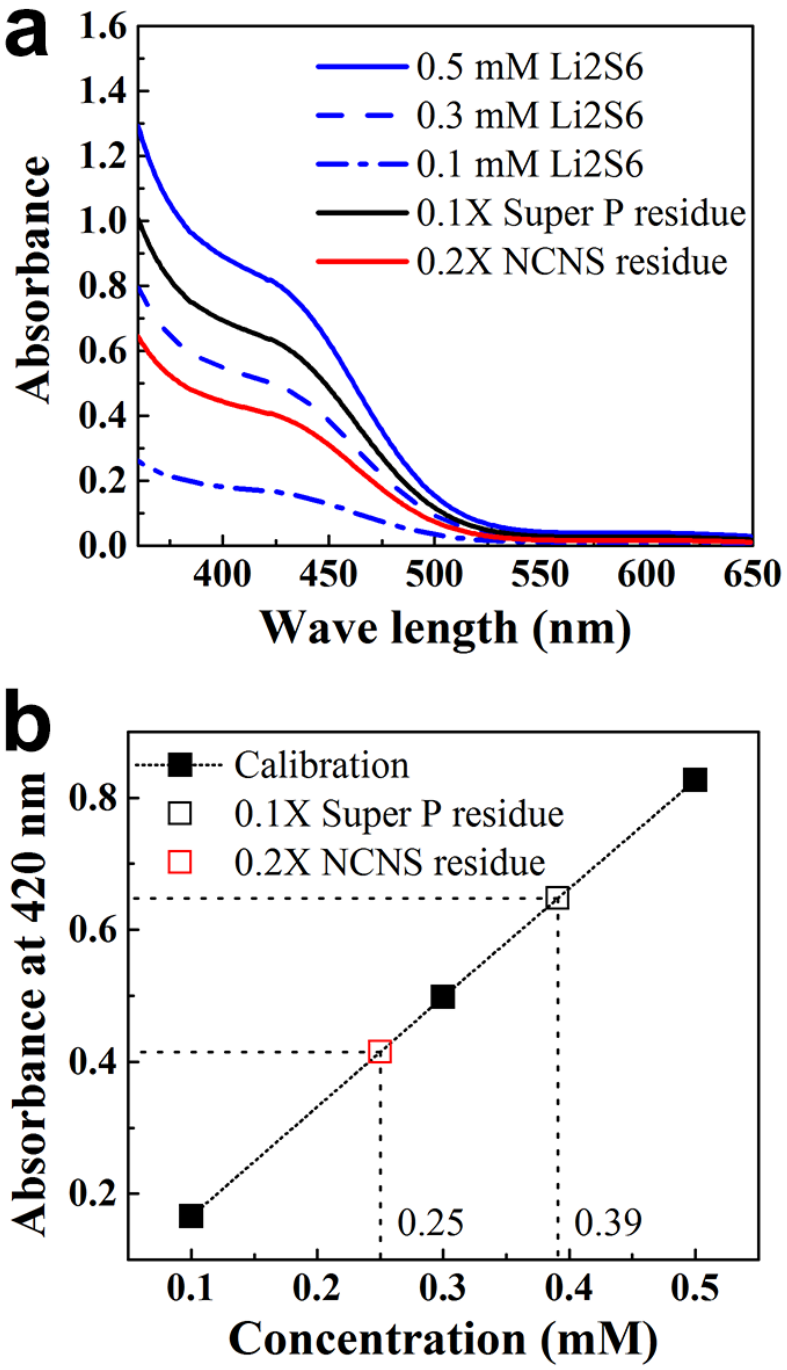

Figure S1. (a) UV-vis spectra of the residue Li_2S_6 solutions after adsorption tests and three calibration solutions. (b) Determination of residue Li_2S_6 concentrations after the adsorption tests.

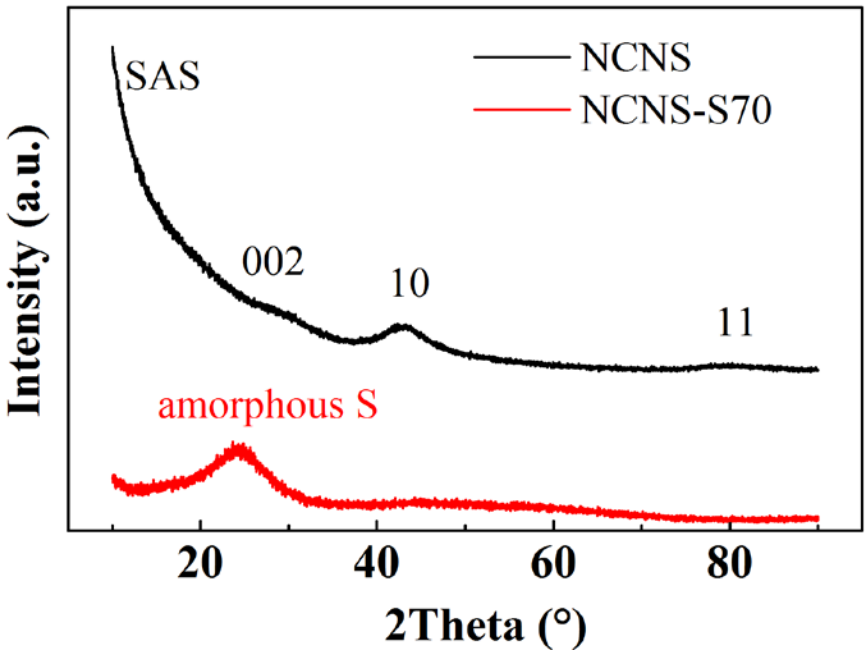

Figure S2. XRD patterns of NCNS and NCNS-S70.

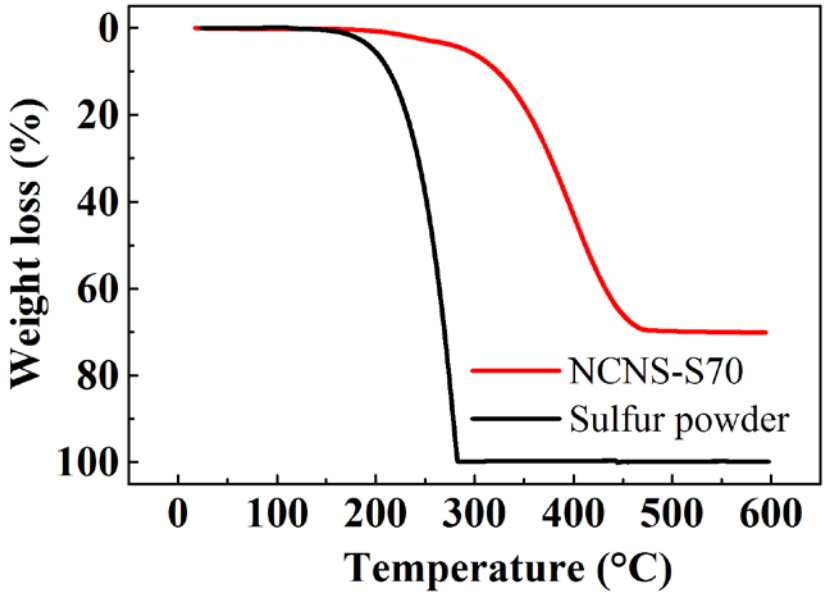

Figure S3. TGA profiles of NCNS-S70 and sulfur powder.

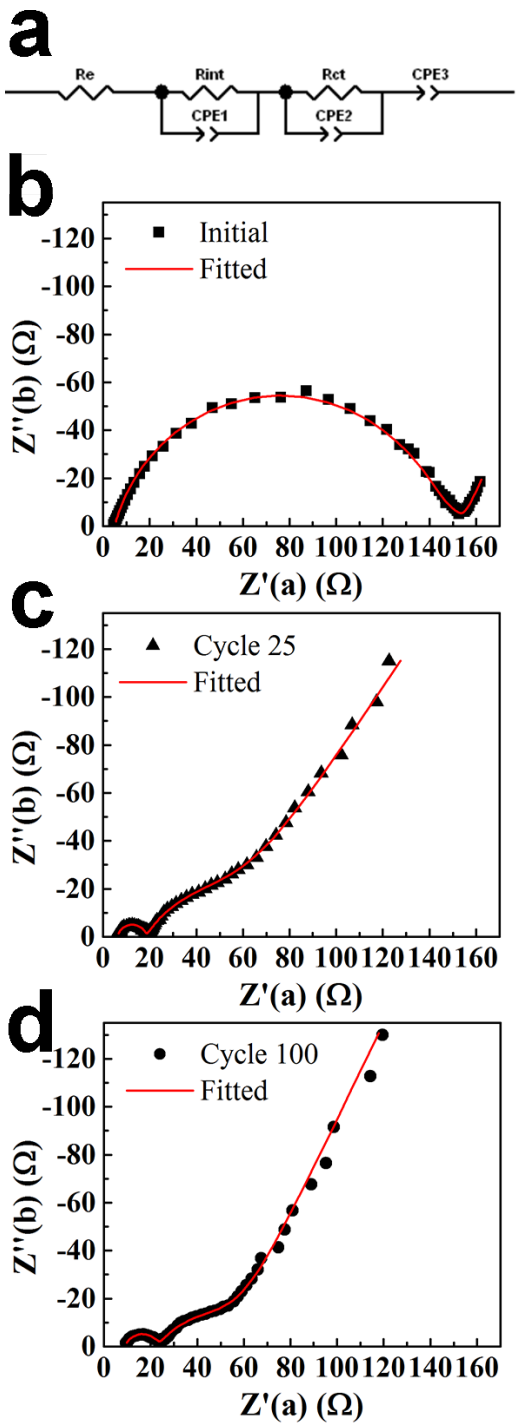

Figure S4. EIS equivalent circuit model[S3] results for the 5 mg cm^{-2} S cell in the charged state: (a) diagrammatic representation of the model; (b) initial state prior to any cycling; (c) after 25 cycles; (d) after 100 cycles.

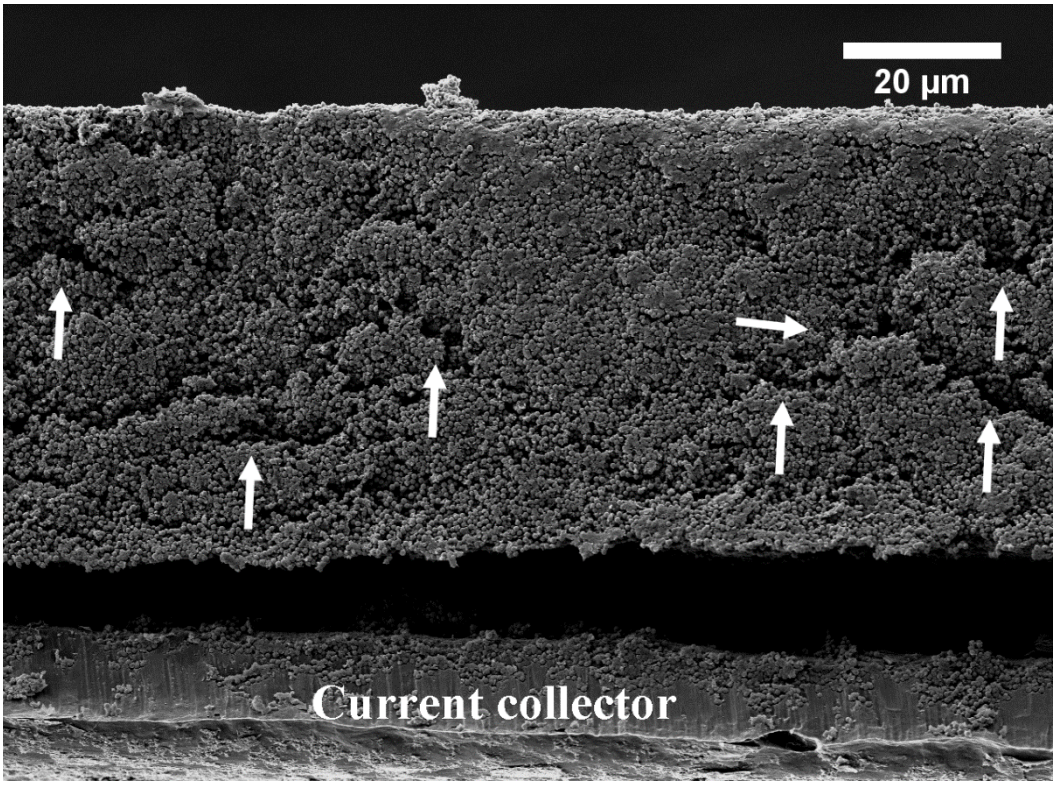

Figure S5. SEM imaging of the cross-sectional morphology of a 5 mg cm^{-2} S thick cathode in discharged state after 25 charge/discharge cycles at 0.2C. The cathode coating maintained its unity after the cycling. Cavities formed in the cathode (see arrows for examples) and it became slightly less dense comparing with the uncycled cathode in the charged state. About 10% expansion of thickness is also observed (~50 µm to ~55 µm). To protect the reactive Li_2S, the cathode for imaging were transferred to the SEM under Ar protection. Epoxy resin was not used for the sectioning. This meant that the current collector separated from the cathode material at the cut edge. The main body of the cathode remained attached to the current collector, however, as witnessed by the absence of charging artefacts.

Table S1. ESI fitted parameters employing the equivalent circuit model shown in Figure S4.

Cycle	Re Ω	Rint Ω	Rct Ω	CPE1-T	CPE1-P	CPE2-T	CPE2-P	CPE3-T	CPE3-P
Initial	5.0	8.1	140.7	1.01E-05	0.83	5.98E-03	0.75	6.56E-02	0.73
25	6.2	12.3	35.8	9.05E-06	0.86	1.03E-02	0.68	3.56E-02	0.63
100	7.0	14.4	33.2	2.20E-05	0.78	8.29E-03	0.63	5.05E-02	0.72

Table S2. Comparison between the 5 mg cm^{-2} S NCNS cell and recently reported high sulfur loading cells.

Reference Number*	d_{cat} µm	A_S mg cm^{-2}	C_S mAh g^{-1}	f_S %	f_{elec} µL mg^{-1}	C_G^{cat} mAh g^{-1}	C_V^{cat} mAh cm^{-3}	W_{ano}** mg	d_{ano}** µm	E_G** Wh kg^{-1}	E_V** Wh L^{-1}
24	160	10.8	900	64	4.9	224.1	607.5	5	95	293.3	763.6
25	300	30.7	825	94	6.8	184.7	844.3	13.1	247.6	220.4	973.1
26	240	10	830	58	10	123.4	345.8	4.3	81.1	152.7	527.5
26	350	20	800	66	10	122.8	457.1	8.3	156.4	148.8	662.4
26	160	6	1200	52	10	173.3	450	3.7	70.4	216.2	620.2
27	1400	9.8	800	83	29	51	56	4.1	76.6	57.9	114.9
28	600	18.1	800	55	14.1	90	241.3	7.5	141.6	108.2	415.6
29	140	4.8	830	55	14.4	92.2	284.6	2.1	38.9	112.7	429.8
29	210	7.2	790	55	11.3	106.1	270.9	2.9	55.6	131.7	430.6
34	110	5	1300	58	10.6	185.1	590.9	3.4	63.5	227	720.2
45	150	5	760	38	6	135	253.3	2	37.1	193.8	394.1
46	100	4.2	1200	66	10	184.2	504	2.6	49.3	226.4	636.2
47	750	17.3	800	54	7	149.6	184.5	7.2	135.3	192.5	334.5
48	360	11.4	900	56	10.5	127.7	285.0	5.3	100.3	157.1	465.1
49	105	5.2	712	66	5	283.1	352.6	1.9	36.2	313.3	490.1
This work	70	5	1100	37	6	192.9	785.7	2.8	53.8	272.7	813.3

* As per main text.

** Projected, see SI text.

References

[S1] Q. Sun, B. He, X. Q. Zhang, A. H. Lu, *ACS Nano* **2015**, 9, 8504.

[S2] J. Song, M. L. Gordin, T. Xu, S. Chen, Z. Yu, H. Sohn, J. Lu, Y. Ren, Y. Duan, D. Wang, *Angew. Chem., Int. Ed. Engl.* **2015**, 54, 4325.

[S3] Z. Deng, Z. Zhang, Y. Lai, J. Liu, J. Li, Y. Liu, *J. Electrochem. Soc.* **2013**, 160, A553.